Acoustic wave scattering by a finite elastic cylinder in water

Jen-Houne Su, Vasundara V. Varadan, and Vijay K. Varadan

Wave Propagation Group, Department of Engineering Mechanics, The Ohio State University, Columbus, Ohio 43210

Lawrence Flax

Naval Research Laboratory, Washington, D.C. 20375
(Received 29 October 1979; accepted for publication 14 April 1980)

Numerical results are obtained for a finite circular elastic cylinder with spherical end caps using Waterman's T-matrix method. In addition to the important practical applications that this geometry has in underwater acoustics, for the first time this method is applied to elastic scatterers that have a discontinuity in the first derivative of the normal to the surface. This makes the problem numerically difficult and is a good test of the effectiveness of the T-matrix method. The frequency dependence of the backscattering cross section is presented for a cylinder whose overall length is twice its diameter. Our results are compared with experiments showing excellent agreement.

PACS numbers: 43.20.Fn, 43.30.Gv, 43.20.Bi

INTRODUCTION

The finite circular cylinder enclosed by spherical end caps is an important model for many applications in underwater acoustics. Many researchers have attempted to study the frequency dependence of a scatterer of this shape submerged in water. Their results are confined to the low-frequency or Rayleigh limit. In this paper the frequency dependence of acoustic wave scattering from a finite elastic cylinder in water is studied using the T-matrix or null field method. To the authors' knowledge such results are unavailable in the literature.

These calculations serve a twofold purpose. The first is that they are of great practical significance, and will be of much use to future experiments on such shapes. The second purpose is of a theoretical and computational nature. For the first time, the T-matrix method has been applied to a three dimensional elastic scatterer whose surface is generated by joining two dissimilar shapes, i.e., there is no single equation governing the surface of the scatterer. Although the normal to the surface which is smooth is continuous, there is a discontinuity in the first derivative of the normal where the hemisphere joins the right circular cylinder. This leads to difficulties in numerical quadrature and matrices that are ill conditioned for inversion. Thus our results are the first real test of the effectiveness of the T-matrix method for elastic scatters. The fact that the elastic scatterer is immersed in water makes the problem more difficult. Waterman[1] has discussed the numerical difficulties associated with electromagnetic scattering from perfectly conducting finite cylinders using this method.

References to theoretical calculations of the problem we are considering are sparse in the literature at wavelengths comparable to the size of the scatterer. The most pertinent work is that of Barnard and McKinney,[2] although it is experimental. They have presented polar plots of the scattered energy from finite solid cylinders and shells. But no direct comparison can be made for two reasons: (1) the cylinders used in experiments have no end caps, (2) the wavelengths they consider are shorter than any that we have considered. The work of Haslett[3] is also experimental on cylinders with no end caps and theoretical estimates of the scattering cross sections are empirical. Williams[4] has considered high-frequency approximations to the finite rigid cylinder whose length is much greater than the wavelength of acoustic waves. Lyamshev[5] has compared experimental results on finite elastic cylinders with theoretical calculations on an infinite cylinder with waves incident obliquely to the axis of the cylinder. Thus, to our knowledge, there are no results available at present for a finite elastic cylinder with spherical end caps at wave lengths comparable to the size of the scatterer.

The T-matrix or null field method originally formulated by Waterman[6] was recently extended to elastic wave scattering by cavities and inclusions in a solid. But the problem of an elastic scatterer in a fluid is far more complicated. Boström[7] was the first to give a correct T-matrix formulation for this case. In Sec. I, we have given a brief summary of the pertinent equations and expressions for the elements of the various matrices that are involved in the definition of the T matrix. In Sec. II the numerical procedure is discussed in sufficient detail and a brief discussion of the numerical results is presented. One of the plots is compared with recently obtained experimental results[8] showing very good agreement.

I. FORMULATION

Consider a finite elastic circular cylinder with hemispherical caps with continuously turning unit normal $\hat{n}$ immersed in an inviscid fluid, see Fig. 1. The elastic properties of the scatterer are given by the Lame's constants λ and μ and mass density ρ while the properties of the fluid are given by the compressibility λ_f and mass density ρ_f.

A plane acoustic wave of unit amplitude, frequency ω and wavenumber k_f is incident obliquely to the cylinder.

 0001-4966/80/080686-06$00.80

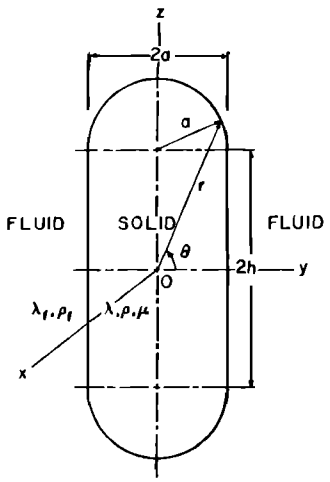

FIG. 1. Geometry of finite circular cylinder with hemispherical end caps.

We denote the incident wave and scattered wave displacements by $\mathbf{u}^0$ and $\mathbf{u}^S$, respectively. The starting point of the T-matrix formalism is the interior and exterior Helmholtz integral representations for the fluid and solid, see Refs. 7 and 9:

$$\mathbf{u}^0(\mathbf{r})+\int_S [\mathbf{u}_f'\cdot(\hat{n}'\cdot\Sigma_f(\mathbf{r},\mathbf{r}'))-\hat{n}'\cdot\tau_f'\cdot\mathsf{G}(\mathbf{r},\mathbf{r}')]\,dS' = \begin{cases}\mathbf{u}_f(\mathbf{r}), & \mathbf{r}\text{ outside }S,\\ 0, & \mathbf{r}\text{ inside }S,\end{cases} \tag{1}$$

for the fluid, and

$$-\int_S [\mathbf{u}'\cdot(\hat{n}'\cdot\Sigma(\mathbf{r},\mathbf{r}'))-\hat{n}'\cdot\tau'\cdot\mathsf{G}(\mathbf{r},\mathbf{r}')]\,dS' = \begin{cases}\mathbf{u}(\mathbf{r}), & \mathbf{r}\text{ inside }S,\\ 0, & \mathbf{r}\text{ outside }S,\end{cases} \tag{2}$$

for the solid, where $\mathbf{u}$ is the displacement vector in the solid, τ is the stress tensor, and Σ and G are the Green's stress and displacement tensors given by

$$\tau=\lambda\mathsf{I}\nabla\cdot\mathbf{u}+\mu(\nabla\mathbf{u}+\mathbf{u}\nabla), \tag{3}$$

$$\Sigma=\lambda\mathsf{I}\nabla\cdot\mathsf{G}+\mu(\nabla\mathsf{G}+\mathsf{G}\nabla), \tag{4}$$

with I is defined as the Idem factor. The terms with subscripts f refer to the corresponding quantities in the fluid and can be written in the form given by (3) and (4) with μ set equal to zero. In Eqs. (1) and (2), the primes on $\mathbf{u}_f$, $\mathbf{u}$, τ_f, τ, and $\hat{n}$ indicate that they are functions of $\mathbf{r}'$, a point on the surface of the finite cylinder S, and dS' is an element of area on S centered at $\mathbf{r}'$. In deriving the above equations, we have assumed that the suitable radiation conditions are imposed on the scattered field far from S.

The philosophy of the T-matrix approach is to expand all the terms appearing in the integral representations in terms of spherical vector basis functions:

$$\psi_{1\sigma mn}(\mathbf{r}) = \left(\frac{k_p}{k_S}\right)^{1/2}\xi_{mn}\nabla\left[h_n(k_p r)P_n^m(\cos\theta)\begin{bmatrix}\cos m\phi, & \sigma=1\\ \sin m\phi, & \sigma=2\end{bmatrix}\right], \tag{5}$$

$$\psi_{2\sigma mn}(\mathbf{r}) = k_S\eta_{mn}\nabla\times\left[\mathbf{r}h_n(k_S r)P_n^m(\cos\theta)\begin{bmatrix}\cos m\phi, & \sigma=1\\ \sin m\phi, & \sigma=2\end{bmatrix}\right], \tag{6}$$

$$\psi_{3\sigma mn}(\mathbf{r})=(1/k_S)\nabla\times\psi_{2\sigma mn}(\mathbf{r}), \tag{7}$$

where $k_p=\omega/c_p$ and $k_S=\omega/c_S$ are the longitudinal (P) and shear wave (S) numbers and c_p and c_S are their respective wave velocities given by

$$c_p=[(\lambda+2\mu)/\rho]^{1/2};\quad c_S=(\mu/\rho)^{1/2}. \tag{8}$$

In Eqs. (5)–(7), we have used spherical polar coordinates r, θ, ϕ with the origin of the coordinate system centered inside S; $h_n(\cdot)$ are the spherical Hankel functions of the first kind of order n; and P_n^m is the associated Legendre polynomial and the index $n=0,1,2,3\cdots\infty$ for $\sigma=1$ and $n=1,2,3\cdots\infty$ for $\sigma=2$, and m is an integer that takes values $0,1,2,3\cdots n$. The symbol σ denotes the even or odd parity of the angular dependence. The normalization constants ξ and η are given by

$$\xi_{mn}=\left[\epsilon_m\frac{(2n+1)(n-m)!}{4\pi(n+m)!}\right]^{1/2} \tag{9}$$

with $\epsilon_0=1$ and $\epsilon_m=2$, $m>0$, and

$$\eta_{mn}=\xi/[n(n+1)]^{1/2}. \tag{10}$$

For brevity, we denote these functions $\psi_{1\sigma mn}$, $\psi_{2\sigma mn}$, $\psi_{3\sigma mn}=\psi_{\tau n}$ with $\tau=1,2,3$. The subscript $\tau=1$ refers to the compressional wave functions while $\tau=2,3$ refers to shear wavefunctions. Since the fluid supports only compressional waves, we need only the $\tau=1$ component of the basis functions which we denote by ψ_{fn}.

We expand the incident wave, scattered wave fields and the field inside the cylinder, and the Green's tensors in terms of the basis functions[7,9]

$$\mathbf{u}^0(\mathbf{r})=\sum_n A_n\,\mathrm{Re}\psi_{fn}(\mathbf{r}), \tag{11}$$

$$\mathbf{u}^S(\mathbf{r})=\sum_n f_n\,\mathrm{Ou}\psi_{fn}(\mathbf{r}), \tag{12}$$

$$\mathbf{u}(\mathbf{r}')=\sum_n \alpha_{\tau n}\,\mathrm{Re}\psi_{\tau n}(\mathbf{r}'), \tag{13}$$

$$\mathsf{G}_f(\mathbf{r},\mathbf{r}')=\frac{ik_f}{\rho_f\omega^2}\sum_n \mathrm{Ou}\psi_{fn}(\mathbf{r}_>)\,\mathrm{Re}\psi_{fn}(\mathbf{r}_<), \tag{14}$$

$$\mathsf{G}(\mathbf{r},\mathbf{r}')=\frac{ik_S}{\rho\omega^2}\sum_{\tau n}\mathrm{Ou}\psi_{\tau n}(\mathbf{r}_>)\mathrm{Re}\psi_{\tau n}(\mathbf{r}_<), \tag{15}$$

where Re and Ou denote regular (j_n) and outgoing (h_n) functions, respectively, and $\mathbf{r}_>$ and $\mathbf{r}_<$ refer to the greater and lesser of $\mathbf{r}$ and $\mathbf{r}'$, respectively. Note that $\mathsf{G}(\mathbf{r}|\mathbf{r}')=\mathsf{G}(\mathbf{r}'|\mathbf{r})$.

Substituting these expansions (11)–(15) and using the following continuity and boundary conditions:

$$\hat{n}'\cdot\mathbf{u}_f'=\hat{n}'\cdot\mathbf{u}', \tag{16}$$

$$\hat{n}'\cdot\tau_f'\cdot\hat{n}'=\hat{n}'\cdot\tau'\cdot\hat{n}', \tag{17}$$

$$(\hat{n}'\cdot\tau')_{\text{tangential}}=0, \tag{18}$$

at the surface of the cylinder in the integral equation for the fluid, Eq. (1), we obtain

$$A_n = -\sum iQ_{n,\tau n'}(\mathrm{Ou},\mathrm{Re})\alpha_{\tau n'}, \tag{19}$$

$$f_n = \sum iQ_{n,\tau n'}(\mathrm{Re},\mathrm{Re})\alpha_{\tau n'}, \tag{20}$$

where the matrix Q is given by

$$Q_{n,\tau n'}\begin{bmatrix}\mathrm{Ou}\\ \mathrm{Re}\end{bmatrix} = \frac{k_f}{\rho_f\omega^2}\int_S \left[\lambda_f\nabla\cdot\begin{bmatrix}\mathrm{Ou}\\ \mathrm{Re}\end{bmatrix}\psi_{fn}\right]\hat{n}\cdot\mathrm{Re}\boldsymbol{\psi}_{f n'} - \hat{n}\cdot\begin{bmatrix}\mathrm{Ou}\\ \mathrm{Re}\end{bmatrix}\psi_{fn}\Big]\hat{n}\cdot\tau(\mathrm{Re}\boldsymbol{\psi}_{\tau n'})\cdot\hat{n}\Big]dS. \tag{21}$$

In Eqs. (19) and (20) and those that follow, the summation sign is used to imply summations on all repeated indices. Obviously, due to summation on τ which varies from 1 to 3, the Q matrix given by (21) has a 1×3 substructure and hence cannot be inverted. Moreover, we have not used the boundary condition as given in Eq. (18). In order to obtain the desired T matrix connecting A_n and f_n, we must invoke Eq. (2) by using an additional expansion

$$\mathbf{u}_f(\mathbf{r}) = \sum_n d_n \mathrm{Re}\boldsymbol{\psi}_{fn}(\mathbf{r}), \quad \mathbf{r}\in S \tag{22}$$

and the conditions given by Eqs. (16)–(18) until we arrive at a set of matrix equations that are invertible. To this end, we follow the work outlined in Refs. 7 and 9 to obtain

$$\sum P_{\tau n,n'}d_{n'} + \sum R_{\tau n,\tau' n'}\alpha_{\tau' n'} = 0, \tag{23}$$

where the matrices P and R are given by

$$P_{\tau n,n'} = \frac{k_S}{\rho\omega^2}\int_S \{(\hat{n}\cdot\mathrm{Re}\boldsymbol{\psi}_{fn'})[\hat{n}\cdot\tau(\mathrm{Re}\boldsymbol{\psi}_{\tau n})\cdot\hat{n}]\}dS, \tag{24}$$

$$R_{\tau n,\tau' n'} = \frac{k_S}{\rho\omega^2}\int_S \{\mathrm{Re}\boldsymbol{\psi}_{\tau' n'})_{\mathrm{tang}}\cdot\hat{n}\cdot\tau(\mathrm{Re}\boldsymbol{\psi}_{\tau n}) - [\hat{n}\cdot\tau(\mathrm{Re}\boldsymbol{\psi}_{\tau' n'})\cdot\hat{n}]\hat{n}\cdot\mathrm{Re}\boldsymbol{\psi}_{\tau n}\}dS. \tag{25}$$

From Eqs. (19), (20), and (23), we then obtain the following relationship between the incident and scattered field coefficients:

$$f = TA, \tag{26}$$

where

$$T = -Q(\mathrm{Re},\mathrm{Re})R^{-1}P[Q(\mathrm{Ou},\mathrm{Re})R^{-1}P]^{-1}. \tag{27}$$

The T matrix defined above is applicable to both elastic and viscoelastic obstacles of arbitrary shape immersed in a fluid.[9] Once the scattered field coefficients are known from Eq. (26), the quantities of interest such as backscattering, bistatic and total scattering cross sections, and amplitude of the scattered field can be computed as a function of the frequency of the incident wave. At distances far from the cylinder, the field consists of outgoing spherical waves with an amplitude that depends on θ and ϕ. The energy carried by the scattered field in any direction defined by the angles (θ,ϕ) is proportional to the absolute square of the scattered pressure amplitude. The farfield scattered amplitude is obtained from Eq. (12) as

$$\mathbf{u}^S(\mathbf{r}) \xrightarrow[|\mathbf{r}|\to\infty]{} \hat{\mathbf{r}}f(\theta,\phi)(e^{ik_f r}/r), \tag{28}$$

where the form function $f(\theta,\phi)$ is given by

$$f(\theta,\phi) = \sum_{n=0}^{\infty}\sum_{m=0}^{n}\xi_{nm}i^{-n}P_n^m(\cos\theta) \times (f_{1mn}\cos m\phi + f_{2mn}\sin m\phi). \tag{29}$$

The differential σ and total σ_t scattering cross sections are given by

$$\sigma(\theta,\phi) = |f(\theta,\phi)|^2, \qquad \sigma_t = \sum_{n=0}^{\infty}\sum_{m=0}^{n}|f_{1mn}|^2 + f_{2mn}|^2. \tag{30}$$

II. NUMERICAL RESULTS

The finite circular cylinder with hemispherical end caps has an axis of revolution which is taken as the z axis of the coordinate system with origin at the center, see Fig. 1. If $2h$ is the length of the cylindrical part and a is the radius of the end caps, the equation to the surface S in spherical polar coordinates (r,θ,ϕ) is given by

$$r(\theta,\phi) = \begin{cases} h\cos\theta + (a^2 - h^2\sin^2\theta)^{1/2}, & 0<\theta<\theta_0,\\ a/\sin\theta, & \theta_0<\theta<\pi-\theta_0,\\ -h\cos\theta + (a^2 - h^2\sin\theta)^{1/2}, & \pi-\theta_0<\theta<\pi, \end{cases} \tag{31}$$

where

$$\theta_0 = \cos^{-1}[h/(a^2+h^2)^{1/2}]. \tag{32}$$

Since $r(\theta,\phi)$ is independent of ϕ, the matrices Q, R, P, and hence T become diagonal in the azimuthal index, i.e.,

$$X_{nm\sigma,n'm'\sigma'} = X^m_{n\sigma,n'\sigma'}\delta_{mm'}, \tag{33}$$

where X stands for Q, R, P, or T. Many more elements of the matrices Q, R, P, and T can be set equal to zero using the additional symmetry

$$r(\theta) = r(\pi-\theta). \tag{34}$$

The above symmetry also makes it possible to reduce the range of integration on θ from $0-\pi$ to $0-\pi/2$, thus saving significant computer time.

The Gauss–Legendre quadrature formula was used to generate the matrix elements. Since the unit normal changes rapidly for $0<\theta<\theta_0$ and remains constant for $\theta_0<\theta<\pi/2$, the integration was divided into two parts and the number of points for each part was varied till convergence was obtained for a given aspect ratio a/h and frequency ω.

The accuracy of the computation was first checked by examining the symmetry of the T matrix in different frequency ranges to determine the proper matrix size. Once this was achieved, the matrix QRP was then inverted by Schmidt orthogonalization. The matrix R was inverted by a Gaussian elimination procedure.

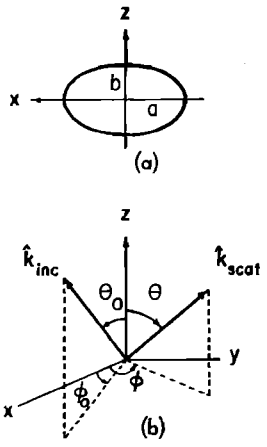

FIG. 2. (a) Geometry of spheroid, (b) scattering geometry.

The matrix sizes for a given azimuthal index m were progressively increased from 8×8 at $k_f(h+a)=0.5$ to 20×20 at $k_f(h+a)=7.0$. For arbitrary angles of incidence with respect to the z axis, it was found that calculating terms up to $m=7$ was sufficient to insure convergence of the solutions.

The input parameters for the program are $k_f h$, a/h, c_f, c_P, c_S, μ, and λ_f and the geometry of the scatterer given by Eq. (31). For the results presented here, a/h was taken to be unity. Thus the overall length of the cylinder is equal to twice the diameter.

The results obtained for the finite cylinder are compared with those for a prolate spheroid, Fig. 2(a), of aspect ratio $b/a=2.0$. Since both are bodies of revolution, the incident wave is taken to be in the x–z plane; see Fig. 2(b). Three incident wave angles $\theta_0=0$, $\pi/4$, and $\pi/2$ were considered with $\phi_0=0$. In each case, the farfield amplitude of the backscattered pressure field $\sqrt{2}f$ (form function) was computed for $\theta=\pi-\theta_0$ and $\phi=\pi$. Figures 3–7 display the form function as a function $k_f l=k_f(h+a)$ for Lucite and aluminum finite cylinders and corresponding results for the prolate spheroid of the same overall dimensions. The material properties used are given in Table I.

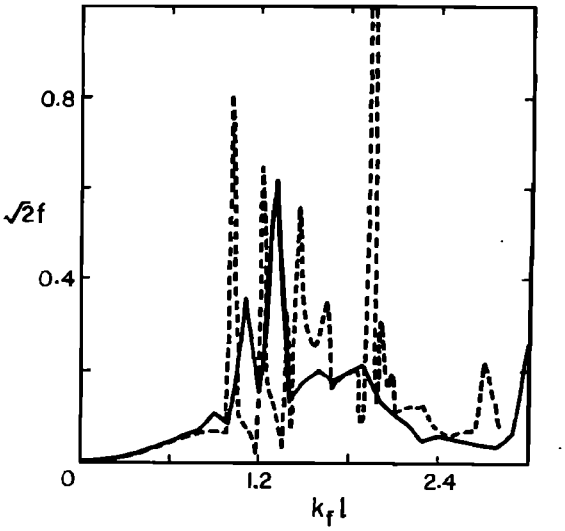

FIG. 4. Form function f as a function of $k_f l$ for Lucite, $\theta_0=45°$; ---spheroid, —finite cylinder.

In Figs. 3–5, the form function is computed in the backscattered direction using the material properties of Lucite, the solid lines indicating the results obtained for the finite cylinder and the dotted lines for the prolate spheroid. The results indicate that the scattering from the spheroid is much more, especially at the maxima which are highly pronounced. Most of the very sharp maxima appear to occur at nearly the same frequency for both scatterers. In contrast, Figs. 6 and 7, using the material properties of aluminum for $\theta_0=0$ and $\pi/2$, respectively, do not display such sharp maxima. At $\theta_0=0$, the curves for the spheroid and the finite cylinder have the same general shape; however the form function has a higher value than that for the spheroid even at the maxima. At $\theta_0=90°$, the form function for both scatterers looks very much alike for the frequency range considered and thus at this angle it is hard to distinguish a finite cylinder from a prolate spheroid. This is not true for all angles of incidence.

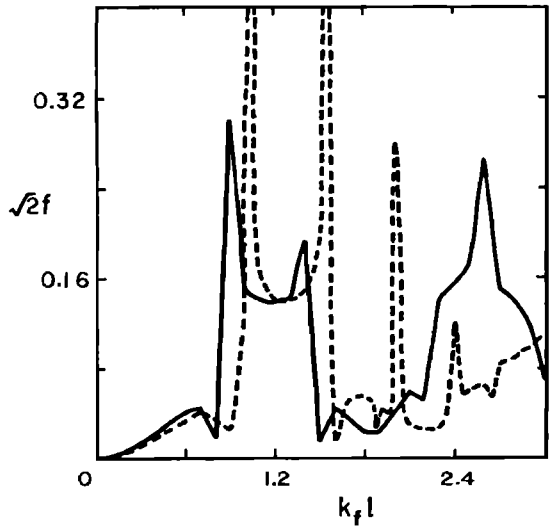

FIG. 3. Form function f as a function of $k_f l$ for Lucite, $\theta_0=0°$; ---spheroid, —finite cylinder.

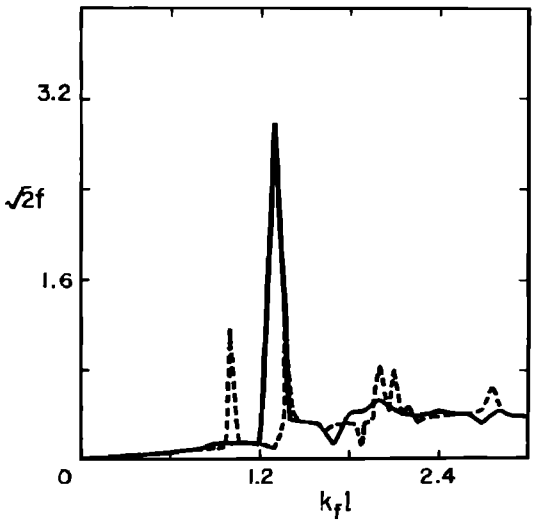

FIG. 5. Form function f as a function of $k_f l$ for Lucite, $\theta_0=90°$; ---spheroid, —finite cylinder.

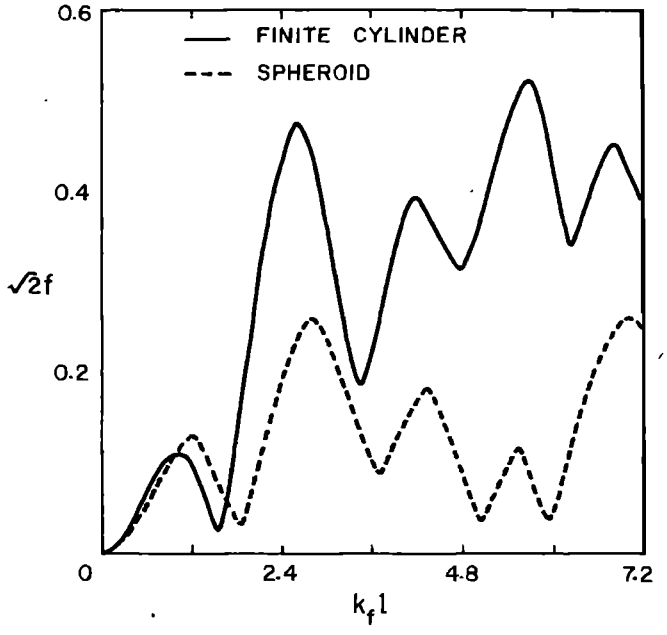

FIG. 6. Form function f as a function of $k_f l$ for aluminum, $\theta_0 = 0°$.

The absence of very sharp maxima in aluminum scatterers may be due to the fact that the shear wave speed in Lucite is quite small and its elastic properties and density are not too far removed from that of water. Thus the wavelength of longitudinal waves is of the same magnitude inside and outside the scatterer. For an aluminum scatterer, the property contrast is quite high and for a given frequency of the incident wave, the wavelength inside the scatterer is smaller than the wavelength in the fluid by a factor of four.

In Fig. 8, our computations are compared with experimental results for end-on incidence for $4.2 < k_f l < 6.6$. Experimental results obtained by Numrich and Dragonette[8] are reliable for $k_f l > 4.6$. The agreement is excellent demonstrating the accuracy of the computations. Twenty terms had to be kept in the scattered field expansion at these frequencies. The experimental results are accurate to ±1 dB and our calculations are within experimental error.

TABLE I. Material properties used in computations.

	Water	Aluminum	Lucite
Density (g/cm^3)	1.00	2.70	1.70
Compressional wave speed ($\times 10^{-5}$ cm/s)	1.482	6.376	2.00
Shear wave speed ($\times 10^{-5}$ cm/s)	0	3.12	0.50

III. CONCLUSIONS

In this paper we have demonstrated that the T-matrix method can be used for elastic obstacles of realistic shape immersed in water for wavelengths comparable to the size of the object. Our calculations also give some indication of where exactly numerical errors become noticeable indicating that our methods for generating the matrix elements by numerical quadrature and matrix inversions should be improved. With our present program calculations can be safely made up to $k_f l = 12$ as long as the cylinder is not too long and thin. For long thin cylinders improvements have to be made in the present procedure to obtain reliable results. The excellent agreement with experiments is nonetheless very encouraging.

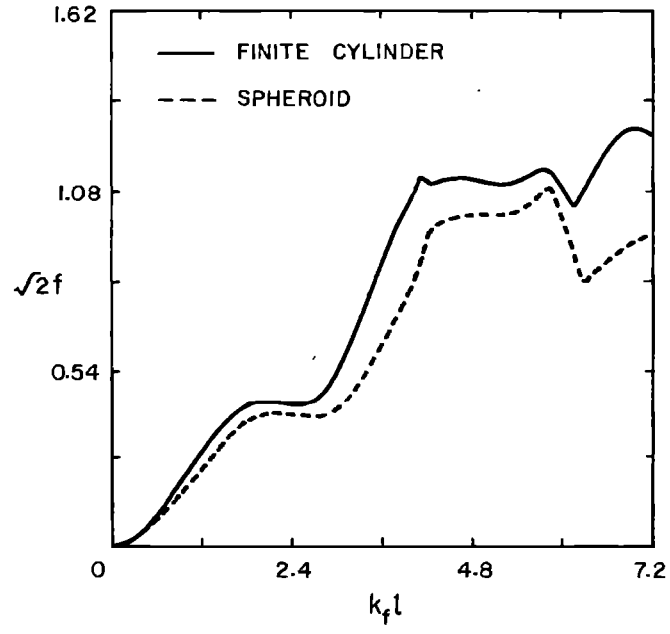

FIG. 7. Form function f as a function of $k_f l$ for aluminum, $\theta_0 = 90°$.

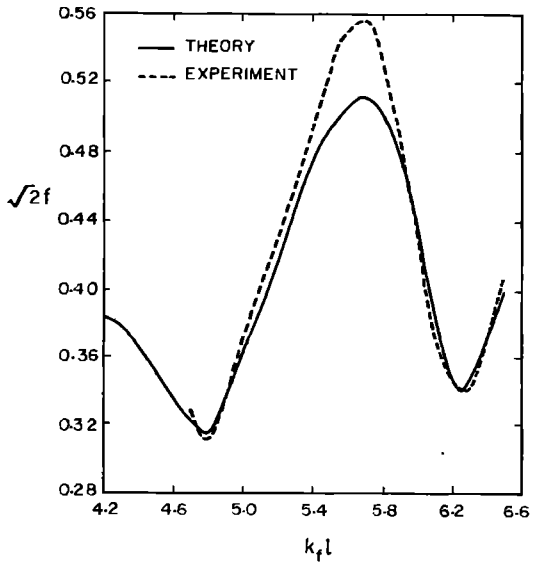

FIG. 8. Backscattered field from an aluminum cylinder for $\theta_0 = 0°$, comparison of theory and experiment.

ACKNOWLEDGMENTS

This work was supported by Naval Research Laboratory under contract N00014-79-C-0859. Helpful discussions with Dr. L. R. Dragonette, Dr. W. Neubauer, and Dr. J. A. Bucaro of NRL, and Dr. B. A. Peterson of OSU are gratefully acknowledged.

[1]P. C. Waterman, Phys. Rev. D 3, 825 (1971).
[2]G. R. Barnard and C. M. McKinney, J. Acoust. Soc. Am. 33, 226 (1961).
[3]R. W. G. Haslett, Brit. J. Appl. Phys. 15, 1085 (1964).
[4]W. E. Williams, Proc. Cambridge Phil. Soc. 52, Pt. 2, 322 (1956).
[5]L. M. Lyamshev, Sov. Phys. Acoust. 5, 56 (1959).
[6]P. C. Waterman, J. Acoust. Soc. Am. 45, 1417 (1969).
[7]A. Boström, J. Acoust. Soc. Am. 67, 390 (1980).
[8]S. Numrich and L. Dragonette (private communication).
[9]B. Peterson, V. V. Varadan, and V. K. Varadan, Int. J. Wave Motion 2, 23 (1980).